Title

Relationship between 7T MR-angiography features of vascular injury and cognitive decline in young brain tumor patients treated with radiation therapy

Journal

Journal of Neuro-Oncology, 153(1)

ISSN

0167-594X

Authors

Avadiappan, Sivakami
Morrison, Melanie A
Jakary, Angela
et al.

Publication Date

2021-05-01

DOI

10.1007/s11060-021-03753-3

Peer reviewed

HHS Public Access

Author manuscript

J Neurooncol. Author manuscript; available in PMC 2022 May 01.

Published in final edited form as:

J Neurooncol. 2021 May ; 153(1): 143–152. doi:10.1007/s11060-021-03753-3.

Relationship between 7T MR–angiography features of vascular injury and cognitive decline in young brain tumor patients treated with radiation therapy

Sivakami Avadiappan[1], **Melanie A. Morrison**[1], **Angela Jakary**[1], **Erin Felton**[2,9], **Schuyler Stoller**[2], **Christopher P. Hess**[1,2], **Annette M. Molinaro**[3,4], **Steve E. Braunstein**[5], **Sabine Mueller**[2,3,6,7], **Janine M. Lupo**[1,8]

[1]Department of Radiology and Biomedical Imaging, University of California, San Francisco, Byers Hall, 1700 4th Street, Suite 303D, Box 2532, San Francisco, CA 94158-2330, USA [2]Department of Neurology, University of California, San Francisco, CA, USA [3]Department of Neurosurgery, University of California, San Francisco, CA, USA [4]Department of Epidemiology and Biostatistics, University of California, San Francisco, CA, USA [5]Department of Radiation Oncology, University of California, San Francisco, CA, USA [6]Department of Pediatrics, University of California, San Francisco, CA, USA [7]University Children's Hospital Zurich, Zurich, Switzerland [8]UCSF/UC Berkeley Graduate Program in Bioengineering, Berkeley and San Francisco, CA, USA [9]Present Address: The George Washington University School of Medicine and Health Sciences, Washington, DC, USA

Abstract

Purpose—Although radiation therapy (RT) is a common treatment for pediatric brain tumors, it is associated with detrimental long-term effects such as impaired cognition, vascular injury, and increased stroke risk. This study aimed to develop metrics that describe vascular injury and relate them to the presence of cerebral microbleeds (CMBs) and cognitive performance scores.

Methods—Twenty-five young adult survivors of pediatric brain tumors treated with either whole-brain (n = 12), whole-ventricular (n = 7), or no RT (n = 6) underwent 7T MRI and neurocognitive testing. Simultaneously acquired MR angiography and susceptibility-weighted images were used to segment CMBs and vessels and quantify their radii and volume.

Results—Patients treated with whole-brain RT had significantly lower arterial volumes (p = 0.003) and a higher proportion of smaller vessels (p = 0.003) compared to the whole-ventricular RT and non-irradiated control patients. Normalized arterial volume decreased with increasing

✉Janine M. Lupo, janine.lupo@ucsf.edu.

Author contribution Study design: JML, SM. Data collection: AJ, EF, SS. Image processing and analysis: SA, MAM. Statistical analysis: SA, AMM, MAM. Data interpretation: JML, SA, SM, AMM, SEB, CPH. Manuscript preparation: SA, MAM, JML. All authors approved the final manuscript content.

All work was performed while at UCSF.

Conflict of interest The authors have no conflict of interest to report with respect to this study.

Ethical approval This study was approved by our institutional review board and performed in accordance with the ethical standards of the institutional and national research committees or comparable ethical standards. Written informed consent, or assent when appropriate, was obtained from all individual participants and additional parental consent was obtained for all minors.

CMB count (R = − 0.66, p = 0.003), and decreasing trends were observed with time since RT and at longitudinal follow-up. Global cognition and verbal memory significantly decreased with smaller normalized arterial volume ($p \leq 0.05$).

Conclusions—Arterial volume is reduced with increasing CMB presence and is influenced by the total brain volume exposed to radiation. This work highlights the potential use of vascular-derived metrics as non-invasive markers of treatment-induced injury and cognitive impairment in pediatric brain tumor patients.

Keywords

MR angiography; Susceptibility-weighted imaging; Late radiation effects; Vascular injury; Cerebral microbleeds; Pediatric brain tumors

Introduction

Brain tumors constitute 26 percent of all childhood cancers [1] and are the most common solid cancer in children under the age of 15 [2]. Radiation therapy (RT) remains a key treatment modality especially for malignant brain tumors. It is typically delivered focally to the primary tumor site either with or without comprehensive cranio-spinal irradiation depending on the specific brain tumor subtype [3]. However, RT is associated with both short- and long-term morbidities [4], especially when RT occurs early in life. Although the onset of vascular changes can occur shortly after RT, late RT-induced toxicities lead to vascular injury, including chronic brain microhemorrhages in the form of cerebral microbleeds (CMBs) [5], cavernous malformations, atherosclerosis, arteriopathies and small vessel occlusive disease [6]. CMBs have been associated with clinical deficits in cognitive performance such as attention, executive function, and working and verbal memory. Large vessel vasculopathies and accelerated atherosclerosis have been linked to increased incidences of neurovascular events such as stroke in pediatric brain tumor survivors [7]. In adults, the presence of CMBs is highly associated with RT dose [5, 8] and time since irradiation [5, 9, 10].

Alterations in vessel radii and vessel volume fraction (defined as the vessel volume normalized by the head volume) have been associated with brain vasculopathies. For example, vessel radii and volume fraction and were shown to be markedly reduced in a group of irradiated rats compared to non-irradiated control animals [11]. The luminal diameter of brain arteries has furthermore been identified as a risk factor for vascular events [12], and as a surrogate marker of arteriopathy in adult patients [13]. In clinical practice, vessel diameters are often visually estimated from MR angiograms, and thus remain highly subjective and dependent on the contrast and resolution of the image. Availability of a more objective criterion would help improve inter-rater agreement and the overall accuracy of diameter estimations. As it has been shown that vascular injury commonly affects small arteries and capillaries [14], we hypothesize that radiation-induced damage to the microvasculature would result in the pruning of small vessels and a shift in vessel radii distribution towards smaller vessel diameters.

Radiation-induced CMBs are lesions corresponding to small hemosiderin deposits from previous episodes of bleeding in the brain related to small vessel damage [15] and are best detected on MRI using SWI [16, 17]. At ultra-high MR field strengths susceptibility contrast is heightened, resulting in enhanced detection, visualization, and quantification of CMBs as well as the surrounding vasculature from which they initially accumulate [5, 18]. Although CMBs have been shown to appear as early as 8 months post-RT and increase in number over time [9, 10, 19], their vascular etiology is still unknown. Thus, investigating CMB location with respect to characteristic changes in the brain vasculature as a result of RT-induced injury is of great interest.

Presence of CMBs have been associated with cognitive decline in pediatric brain tumor survivors treated with RT [19]. CMBs have also been associated with cognitive decline in patients with cerebral cavernous malformations [20], traumatic brain injuries [21], and healthy aging adults [22]. Given the natural history of CMBs in relation to the vasculature, it is hypothesized that arterial vessel properties such as radii and volume fraction would evolve with CMB formation and similarly explain the cognitive status of irradiated patients. Understanding the extent of vascular damage as well as identifying additional metrics that are both associated with cognitive performance and represent unique features of radiation-induced vascular injury will also be helpful in generating future predictive models of cognitive decline in this population. The goals of this study were to (i) quantify vessel radii and volume fraction in order to evaluate the severity of RT-induced injury, (ii) examine the effects of CMB presence on the surrounding vascular structure, and (iii) relate vessel metrics to verbal memory, executive function and global performance.

Materials and methods

Study population

Imaging and cognitive data were acquired from nineteen patients with brain tumors (ages 10–25 years, median 17 years) treated with either photon-based whole brain RT (WBRT; n = 12) or whole ventricular RT (WVRT; n = 7) 0.1–19.9 years prior (median 3.29 years). Patients were recruited from a larger multisite prospective trial called “Radiation-induced Arteriopathy and Stroke Risk in Children with Cancer treated with Cranial Radiation Therapy” (RadArt) in childhood brain tumor survivors. The study was approved by our institutional review board. Written informed consent, or assent when appropriate, was obtained for all patients and their guardians if patients were under the age of 18.

Inclusion criteria for the RT groups included treatment with RT at age < 25 years, completion of treatment at least 1 month prior to enrollment, age > 6 and < 30 at time of assessment, and ability to undergo an MRI without sedation. A set of six nonirradiated control patients (ages 13–16 years) were also recruited. Exclusion criteria for all groups consisted of known vasculopathy prior to initiation of RT, the presence of a shunt, medications affecting neurocognitive status and co-morbid disorders that affect cognition (e.g. history of developmental delay, neurofibromatosis 1, and hydrocephalus) as determined by the treating physician. Ten patients, including two non-irradiated controls, returned for follow-up cognitive testing and imaging 0.9–3.7 years (median 1.3 years) following their initial visit.

Cognitive assessment

Prior to the research MRI, subjects completed a computerized battery of neurocognitive tests (Cogstate, Inc.; New Haven, CT) [23], to evaluate multiple domains of cognitive function including executive function measured via the Groton Maze Learning (GML) test and verbal memory measured via the International Shopping List (ISL) test. In the GML test, users were instructed to discover a hidden maze in a matrix of boxes; in the ISL test, users were repeatedly presented with a word list and instructed to freely recall the shopping items. These tasks were selected for this analysis because they have been previously related to imaging findings [19, 24]. The other cognitive domains and tests adminitstered in the battery included attention (Identification Task (IDN)), association learning and visual memory (Continuous Paired Associate Learning Task (CPAL)), psychomotor function (Detection Task (DET)), Delayed Recall for ISL (ISRL)), and working memory (One Back Test (ONB)). Normalized age-appropriate z-scores were derived from mean performance scores of healthy control subjects from the Cogstate database. A global performance score was generated for each patient by averaging z-scores from all the seven tests.

Image acquisition

All patients were imaged using a 7T MRI scanner (GE Healthcare, Wisconsin) with a 32-channel phased-array coil (NOVA Medical, Massachusetts). A four-echo, gradient echo sequence [25] with TOF capability for the first echo was acquired, enabling simultaneous imaging of the arteries, veins, and CMBs, while obviating the need for image co-registration and reducing the total scan time. Imaging parameters for the TOF-MRA-SWI sequence included: flow compensation along readout, repetition time (TR)/echo time (TE)/TE2/TE3/TE4 = 40/2.7/10.5/13.2/20.9 ms, flip angle (FA) = 25°, with 1 mm slice thickness, 0.5 mm in-plane resolution, 24 cm field of view (FOV).

Post processing

Raw k-space data from the 32 coils were transferred off-line to a Linux workstation where image reconstruction and post-processing was performed using in-house programs written with MATLAB software. Magnitude images from each coil were then combined using the root sum of squares and skull stripping was performed using FMRIB Software Library (FSL)’s Brain Extraction Tool (BET) [26]. The magnitude images from the first echo were used for MRA and the final three echoes were used for SWI processing as described in Bian et al. [25].

Image pre–processing

The TOF-MRA and SWI were first resampled to 0.23 mm isotropic resolution using bi-cubic interpolation and intensity normalized. Overlapping 2D maximum intensity projections and minimum intensity projections were obtained for the MRA and SWI, respectively, by taking projections through 8 mm along the superior-inferior direction. Vessel segmentation was performed on the 8 mm projected image using a novel algorithm that improves on the Hessian-based Frangi filter [28].

Vessel segmentation algorithm

The mathematics behind the Hessian-based Frangi filter for the purpose of vessel segmentation has been previously presented [28]. In brief, a multiscale Hessian matrix describing the local curvature along each vessel and its respective cross-section is obtained by taking the second partial derivative of the maximum intensity projected image. The eigenvalues are extracted from the Hessian matrix and based on the relationship between eigenvalues, the likelihood of tube-like structures is determined. As the human cerebral vasculature covers multiple radii ranges, multi-scale smoothing is required to generate the final segmented image. This is typically achieved using multiple runs of a Gaussian filter, each with a different sigma value. Although the Frangi vessel enhancement method is an excellent technique for visualization, the accuracy of radii of vessels is not preserved due to the use of a uniform multi-scale filtering approach.

We implemented an algorithm previously described by Avadiappan et al. [27] that builds upon the Frangi vessel enhancement method, providing the vessel enhancement feature with the advantage of maintaining accurate vessel shape for improved radii estimates. The algorithm automatically determines the appropriate set of filter scales for each vessel by first calculating the radii of large vessels using intensity-based thresholding followed by discrete distance transforms. From the output of the adaptive Frangi filter, Fast Marching [29] with an intensity threshold of 0.001 was performed on each of the maximum intensity projected images to obtain the binary image. A similar approach was used to segment the veins from SWI (Fig. 1a, b).

Vessel radii estimation

A 2D Euclidean distance transform (EDT) map, which labels each pixel of the image with the distance to the nearest boundary pixel, was obtained from the binary image. Voxel-wise measures of vessel radii were generated by employing a thinning procedure to first obtain the vessel skeleton of the binary image, followed by multiplication of the 2D EDT with the vessel skeleton to obtain a final vessel radii map. Histograms of the vessel radii map were then generated to depict vessel radii distribution in the MIP slice (Fig. 1e). The total arterial volume was then computed from non-overlapping 8 mm projections through the entire brain. The total arterial volume was normalized by the head volume to generate the normalized vessel volume. The proportion of small vessels to the total number of small, medium and large vessels was then compared with time since RT, number of CMBs, and cognitive scores for each sex and type of RT. Serial changes were evaluated in the patients with repeat scans. Since vessel radii can vary with sex [30], the normalized vessel distribution was obtained separately for males and females. The volume of the segmented veins and venous vessel radii were not computed because of the known fluctuations in venous diameter with changes in oxygenation.

Vessel–CMB distance

CMBs were detected using a semiautomated CMB detection algorithm [31]. The algorithm accepts a stack of SWI images and identifies all putative CMB candidates before using feature extraction and user input to identify true CMBs from hard mimics associated with veins. The segmented arteries from MRA, veins from SWI, and detected CMBs were

overlaid on a single image for better visualization (Fig. 1c, d). From the skeleton of the segmented arteries and veins, the nearest vessel endpoints with respect to each CMB were automatically determined (Fig. 1f–h). The distance between the individual CMB centroids and the nearest artery and vein ending was computed. The relationship between CMB volume and their respective distance to a neighboring vessel were evaluated; and the distance to the nearest artery was also compared to the distance from the nearest vein.

Regional analyses

In order to quantify the regional distribution of arteries in the lobes, the Montreal Neurological Institute (MNI) lobar template was first registered to the unprocessed 3D TOF image data using the T1-weighted anatomical image data as an intermediate registration volume. Following this, 8 mm projections were obtained for all four lobar regions and vascular metrics were calculated. The regional arterial volumes were compared among the different treatment groups (i.e. WBRT, WVRT, no RT).

Statistical analyses

Global and local normalized vessel volume and proportion of small vessels were compared among the different treatment groups using a Kruskal–Wallis test for significance. Generalized linear models with normalized arterial vessel volume and proportion of small vessels as outcomes were modelled with treatment type as the input after controlling for age, sex and time since treatment. Age-normalized z-scores from three cognitive tests and the cumulative global performance z-score were correlated with each vascular metric using a Pearson correlation coefficient.

Results

Patient demographics are listed in Table 1. Three non-irradiated patients were excluded from the analysis due to the presence of hydrocephalus and one medulloblastoma patient was excluded due to severe head motion, resulting in 10 patients in the WBRT group, 7 in the WVRT group and 4 in the nonirradiated control group.

The group differences for time since RT and age at RT are shown in Fig. 2a, d with the WVRT irradiated group being slighly older compared to the WBRT group ($p = 0.058$). Overall, normalized arterial vessel volume decreased as a function of time since RT ($R = -0.39$, $p = 0.13$), and CMB count ($R = -0.66$, $p = 0.003$) (Fig. 2b, c). Individuals after WBRT presented with significantly lower vessel volumes compared to the WVRT group and the control group with no RT ($p = 0.003$; Fig. 2e). Multiple regression analysis was performed and after controlling for age, sex and time since RT, normalized arterial vessel volume was still significantly associated with the type of RT ($p = 0.007$), with smaller arterial vessel volumes observed in patients with larger irradiated volumes. The normalized arterial vessel volume decreased on average, by 5% in 5 out of the 6 irradiated patients during the follow-up scan compared to baseline (Fig. 2f).

The local arterial vessel volume normalized by the regional volume reduced uniformly across all four lobes for patients who received WBRT compared to the no RT group; whereas, for patients who received WVRT, the arterial volume reduced only in occipital and

temporal lobes, suggesting that the vascular effects of RT depend on the regions irradiated (Fig. 3a). When individual lobes were grouped as non-irradiated vs. irradiated, the irradiated lobes consistently exhibited lower normalized vessel volume compared to the non-irradiated areas (Fig. 3b–e).

Analysis of the cognitive data revealed that the global performance and verbal memory measured by the ISL test increased with elevated normalized arterial volume, with p values of 0.05 and 0.007, respectively (Fig. 4a, b). The GML test score of executive function showed a similar trend that did not reach statistical significance (Fig. 4c). In patients with follow-up scans, the rate of change of ISL scores increased linearly with respect to rate of change of normalized vessel volume ($r = 0.86$, $p = 0.03$) as shown in Fig. 4d.

Patients with WBRT exhibited a significantly higher proportion of small arterial vessels (0.23–0.46 mm in diameter) compared to patients who received WVRT and patients with no RT ($p = 0.003$). Similar to normalized arterial vessel volume, the proportion of small arteries was also found to be significantly associated with the type of RT ($p < 0.05$) when controlling for age, sex and time since treatment, with an increasing number of smaller arteries found with larger RT treatment volumes. The normalized proportion of small vessels increased on average by 20% in 5 out of the 6 patients during the follow-up scan compared to baseline and with respect to time since RT for both males and females. No obvious trends were noted in the medium (0.46–0.92 mm) and large radii (0.92–1.84 mm) vessel counts (Fig. 5a–c).

The majority of CMBs were located closer to veins than arteries (Fig. 5d, e), regardless of RT type. Although larger CMBs were initially farther away from the nearest vein, with longer times since RT, CMBs far from surrounding vasculature varied in size as shown in Fig. 5f.

Discussion

Despite the known risk of brain injury following RT, our understanding of these changes in cerebral vasculature is limited. Since the survival rates for pediatric brain tumors have significantly increased during the last decades, investigating the long-term therapy-related sequelae are of high importance. In an effort to evaluate cerebrovascular sequelae after RT treatment in patients with pediatric brain tumors, we investigated 25 survivors using SWI and MRA. Although MRA has previously been used to investigate morphological changes in the vasculature resulting from treatment for brain metastases [32], to our knowledge this is the first study to use MRA at 7T in a quantitative manner to evaluate treatment-related changes in the cerebral vasculature of childhood brain tumor survivors. Although this study was performed at 7T to provide enhanced detection of CMBs and small vessels due to elevated susceptibility contrast and SNR that can be used to increase resolution, the sequences and analysis methods employed can now easily be expanded to lower field strength data for routine clinical use.

One of the primary findings of this work highlights the reduction of arterial vessel volume that results following RT, an effect that persists for many years after receiving RT and is influenced by the total brain volume exposed to radiation as evident in the WBRT group

which presented with the lowest vessel volumes. Pathologically, this observation could be caused by RT-induced vascular atrophy or pruning of smaller vessels, aligning with our longitudinal finding of an increased proportion of vessels with small radii. A previous study has demonstrated that patients treated with RT at least 1 year prior had one or more CMBs, and that non-irradiation control patients had none [24]. As expected, our current work identified a relationship between changes in vessel volume and the development of CMBs, affirming that these phenomena are related and co-evolving, and that the metrics can be used to describe the overall integrity of the vasculature after radiation treatment. No correlations were found between our vascular metrics and type or dose of concomitant or adjuvent chemotherapy received. We also demonstrate that these metrics can accurately describe the cognitive status of individual patients, given the relationship observed between arterial vessel volume and both verbal memory and global cognitive performance that could also not be attributed to differences in chemotherapy. The closeness of CMBs to veins rather than arteries may suggest that after a CMB forms, the surrounding vasculature narrows and eventually recedes. This hypothesis also aligns with our prior hypothesis that vessel volume is decreasing due to simultaneous atrophy or pruning of vasculature.

A few factors have limited our progress, including limited sample size and longitudinal follow-up scans as well as some heterogeneity of patient characteristics. Although more consistent and longer follow-up times will help uncover the full scope of RT induced cerebrovascular changes in this high risk population, this is the first application of vessel metrics from MRA for this application and paves the way for more refined research with larger sample sizes. The potential contributions of age at diagnosis could not be ruled out in this analysis since the brain undergoes maturational development from childhood to adolescence. Integration of radiation dosimetry maps would also be useful in determining the exact radiation dose applied to individual brain voxels as to appropriately assess associations between treatment volume and vascular changes. Although our limited sample size precluded us from quantifying the effects of whole brain dose on arterial metrics, we observed that 3 of the 4 higher risk medulloblastomas who received a whole brain dose of 36 Gy had reduced arterial vessel volume compared to those who received a 24 Gy whole-brain dose. Ultimately, the vascular metrics described in our paper have the potential to aid in novel mitigation strategies for RT-induced cognitive decline, such as cognitive rehabilitation therapy or treatment with a drug like memantine that can decelerate cognitive impairment.

Conclusion

In conclusion, using SWI and MRA, we have demonstrated that arterial radii changes occur with a high prevalence after RT in patients with pediatric brain tumors and are associated with irradiated volume and CMB count, and trend with longer follow-up time. This preliminary work highlights the potential for arterial vessel radii to be used in conjuntion with CMB burden as non-invasive markers of treatment-induced vascular injury and cognitive impairment in this vulnerable population.

Acknowledgements

This work was supported by NIH-NICHD grant RO1HD079568 and funding from the La Roche family. We thank all the patients and families for their participation in this study.

References

1. https://www.cancer.org/cancer/cancer-in-children/types-of-childhood-cancers.html
2. https://www.childrensoncologygroup.org/index.php/braintumors
3. Knab B, Connell PP (2007) Radiotherapy for pediatric brain tumors: when and how. Expert Rev Anticancer Ther 7(sup1):S69–S77 [PubMed: 18076312]
4. Taphoorn MJ, Klein M (2004) Cognitive deficits in adult patients with brain tumors. Lancet Neurol 3(3):159–168 [PubMed: 14980531]
5. Lupo JM, Chuang CF, Chang SM, Barani IJ, Jimenez B, Hess CP, Nelson SJ (2012) 7-Tesla susceptibility-weighted imaging to assess the effects of radiotherapy on normal-appearing brain in patients with glioma. Int J RadiatOncolBiolPhys 82(3):e493–500
6. Greene-Schloesser D, Robbins ME, Peiffer AM, Shaw EG, Wheeler KT, Chan MD (2012) Radiation-induced brain injury: a review. Front Oncol 2:73 [PubMed: 22833841]
7. Campen CJ, Kranick SM, Kasner SE et al. (2012) Cranial irradiation increases risk of stroke in pediatric brain tumor survivors. Stroke J CerebCirc 43(11):3035–3040
8. Wahl M, Anwar M, Hess CP, Chang SM, Lupo JM (2017) Relationship between radiation dose and microbleed formation in patients with malignant glioma. RadiatOncol 12(1):12
9. Lupo JM, Molinaro AM, Essock-Burns E, Butowski N, Chang SM, Cha S, Nelson SJ (2016) The effects of anti-angiogenic therapy on the formation of radiation-induced microbleeds in normal brain tissue of patients with glioma. NeuroOncol 18(1):87–95
10. Morrison MA, Hess CP, Clarke JL, Butowski N, Chang SM, Molinaro AM, Lupo JM (2019) Risk factors of radiotherapy-induced cerebral microbleeds and serial analysis of their size compared with white matter changes: A 7T MRI study in 113 adult patients with brain tumors. J MagnReson Imaging 50(3):868–877
11. Deshpande SS, Donneys A, Farberg AS, Tchanque-Fossuo CN, Felice PA, Buchman SR (2014) Quantification and characterization of radiation-induced changes to mandibular vascularity using micro-computed tomography. Ann PlastSurg 72(1):100–103
12. Gutierrez J, Cheung K, Bagci A et al. (2015) Brain arterial diameters as a risk factor for vascular events. J Am Heart Assoc 4(8):e002289 [PubMed: 26251284]
13. Mazighi M, Labreuche J, Gongora-Rivera F, Duyckaerts C, Hauw JJ, Amarenco P (2009) Autopsy prevalence of proximal extracranial atherosclerosis in patients with fatal stroke. Stroke 40(3):713–718 [PubMed: 19118247]
14. Roth NM, Sontag MR, Kiani MF (1999) Early effects of ionizing radiation on the microvascular networks in normal tissue. Radiat Res 151(3):270–277 [PubMed: 10073664]
15. Cole FM, Yates P (1967) Intracerebralmicroaneurysms and small cerebrovascular lesions. Brain 90:759–768 [PubMed: 6075809]
16. Haacke EM, Xu Y, Cheng YC, Reichenbach JR (2004) Susceptibility weighted imaging (SWI). MagnReson Med 52(3):612–618
17. Lupo JM, Banerjee S, Hammond KE, Kelley DA, Xu D, Chang SM, Vigneron DB, Majumdar S, Nelson SJ (2009) GRAPPA-based susceptibility-weighted imaging of normal volunteers and patients with brain tumor at 7 T. MagnReson Imaging 27(4):480–488
18. Bian W, Hess CP, Chang SM, Nelson SJ, Lupo JM (2014) Susceptibility-weighted MR imaging of radiation therapy-induced cerebral microbleeds in patients with glioma: a comparison between 3T and 7T. Neuroradiology 56(2):91–96 [PubMed: 24281386]
19. Roddy E, Sear K, Felton E et al. (2016) Presence of cerebral microbleeds is associated with worse executive function in pediatric brain tumor survivors. NeuroOncol 18(11):1548–1558
20. Akers A, Al-Shahi Salman R, Awad IA et al. (2017) Synopsis of guidelines for the clinical management of cerebral cavernous malformations: consensus recommendations based on systematic literature review by the angioma alliance scientific advisory board clinical experts panel. Neurosurgery 80:665–680 [PubMed: 28387823]
21. Salehi A, Zhang JH, Obenaus A (2017) Response of the cerebral vasculature following traumatic brain injury. J Cereb Blood Flow Metab 37(7):2320–2339 [PubMed: 28378621]

22. Poels MMF, Ikram MA, Van Der Lugt A, Hofman A, Niessen WJ, Krestin GP, Breteler MM, Vernooij MW (2012) Cerebral microbleeds are associated with worse cognitive function: the rotterdam scan study. Neurology 78(5):326–333 [PubMed: 22262748]

23. Maruff P, Thomas E, Cysique L et al. (2009) Validity of the CogState brief battery: relationship to standardized tests and sensitivity to cognitive impairment in mild traumatic brain injury, schizophrenia, and AIDS dementia complex. Arch ClinNeuropsychol 24(2):165–178

24. Morrison MA, Mueller S, Felton E et al. (2021) Rate of radiation-induced microbleed formation on 7T MRI relates to cognitive impairment in young patients treated with radiation therapy for a brain tumor. Radiother Oncol 154(1):145–153 [PubMed: 32966846]

25. Bian W, Banerjee S, Kelly DA et al. (2015) Simultaneous imaging of radiation-induced cerebral microbleeds, arteries and veins, using a multiple gradient echo sequence at 7 Tesla. J MagnReson Imaging 42(2):269–279

26. Smith SM (2002) Fast robust automated brain extraction. Ann Meet Organ Hum Brain Mapp 17(3):143–155

27. Avadiappan S, Payabvash S, Morrison MA et al. (2020) A fully automated method for segmenting arteries and quantifying vessel radii on magnetic resonance angiography images of varying projection thickness. Frontiers Neurosci Brain Imaging Methods 14:537

28. Frangi AF, Niessen WJ, Vincken KL, Viergever MA (1998) Multiscale vessel enhancement filtering. In: Proceedings of medical image computing and computer-assisted intervention (MICCAI.), pp 130–137

29. Sethian JA (1996) A fast marching level set method for monotonically advancing fronts. ProcNatlAcadSci USA 93(4):1591–1595

30. Bullitt E, Zeng D, Mortamet B et al. (2010) The effects of healthy aging on intracerebral blood vessels visualized by magnetic resonance angiography. Neurobiol Aging 31(2):290–300 [PubMed: 18471935]

31. Bian W, Hess CP, Chang SM, Nelson SJ, Lupo JM (2013) Computer-aided detection of radiation-induced cerebral microbleeds on susceptibility-weighted MR images. NeuroimageClin 2(1):282–290

32. Bullitt E, Lin NU, Smith KJ et al. (2009) Blood vessel morphological changes as visualized by MRA during treatment of brain metastases: a feasibility study. Radiology 245(3):824–830

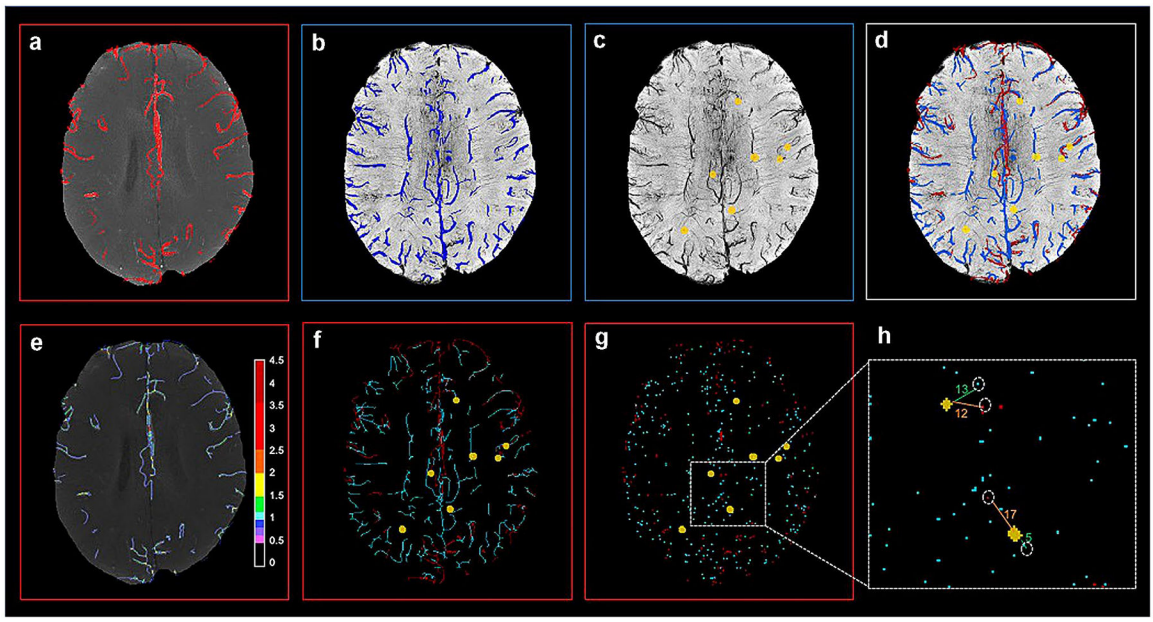

Fig. 1.

Overlay of segmented arteries, veins and microbleeds from corresponding 8 mm projected slice (top) and steps in vessel-CMB distance calculation (bottom); **a** Segmented arteries overlaid on MRA; **b** Segmented veins overlaid on SWI; **c** Segmented CMBs overlaid on SWI; **d** Combined display of arteries, veins, CMBs; **e** Vessel radii map overlaid on MRA (color bar scale in number of pixels); **f** Artery and vein skeleton with CMBs; **g** Vessel end points with CMBs; **h** CMB- nearest vessel distance

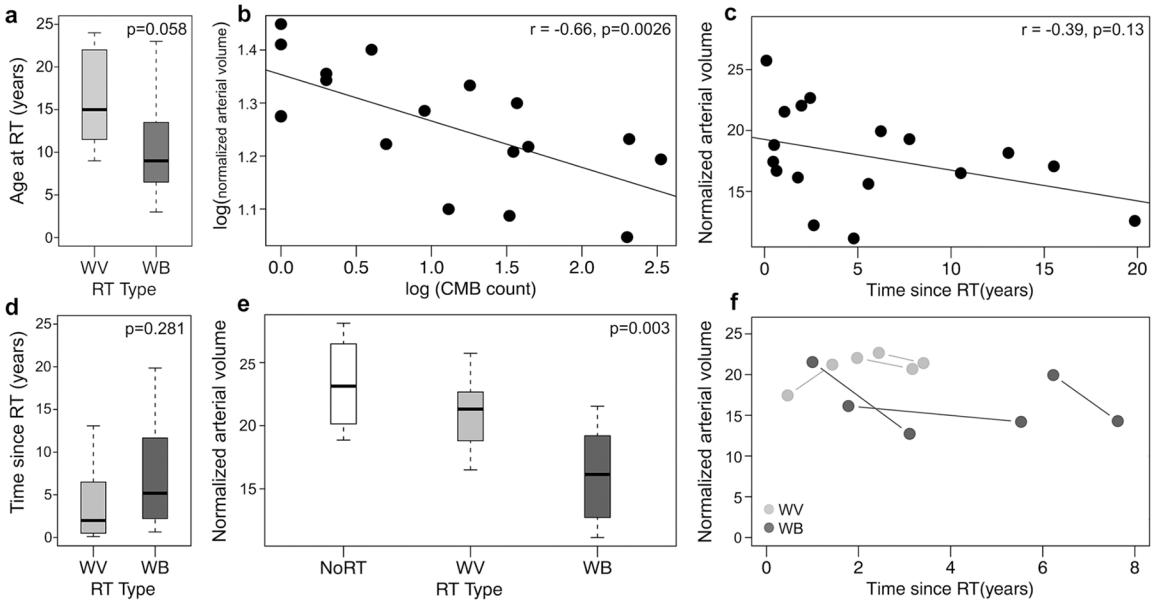

Fig. 2.

a Difference in age between the whole ventricular (WV) and whole brain (WB) RT groups; **b** Logarithmic plot between normalized arterial volume and number of CMBs; **c** Normalized arterial volume as a function of time since RT; **d** Difference in time since RT between WB and WV treatment groups; **e** Distribution of normalized vessel volume in the different treatment groups; **f** Longitudinal differences in arterial volume in the patients with serial scans

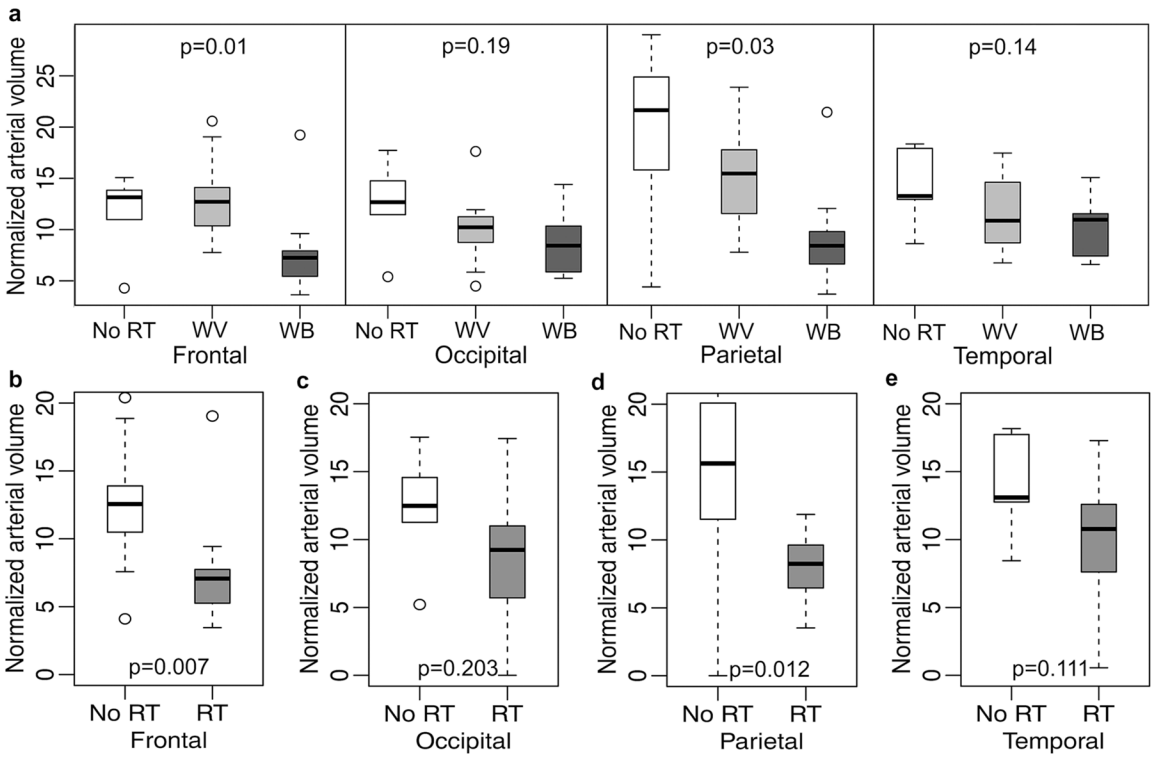

Fig. 3.

a Normalized arterial volume in different brain lobes for no RT, whole ventricular (WV) and whole brain (WB) RT groups; **b–e** Normalized arterial volume stratified by irradiated and non-irradiated regions of the brain. For the WVRT group, only the occipital and temporal lobes were irradiated

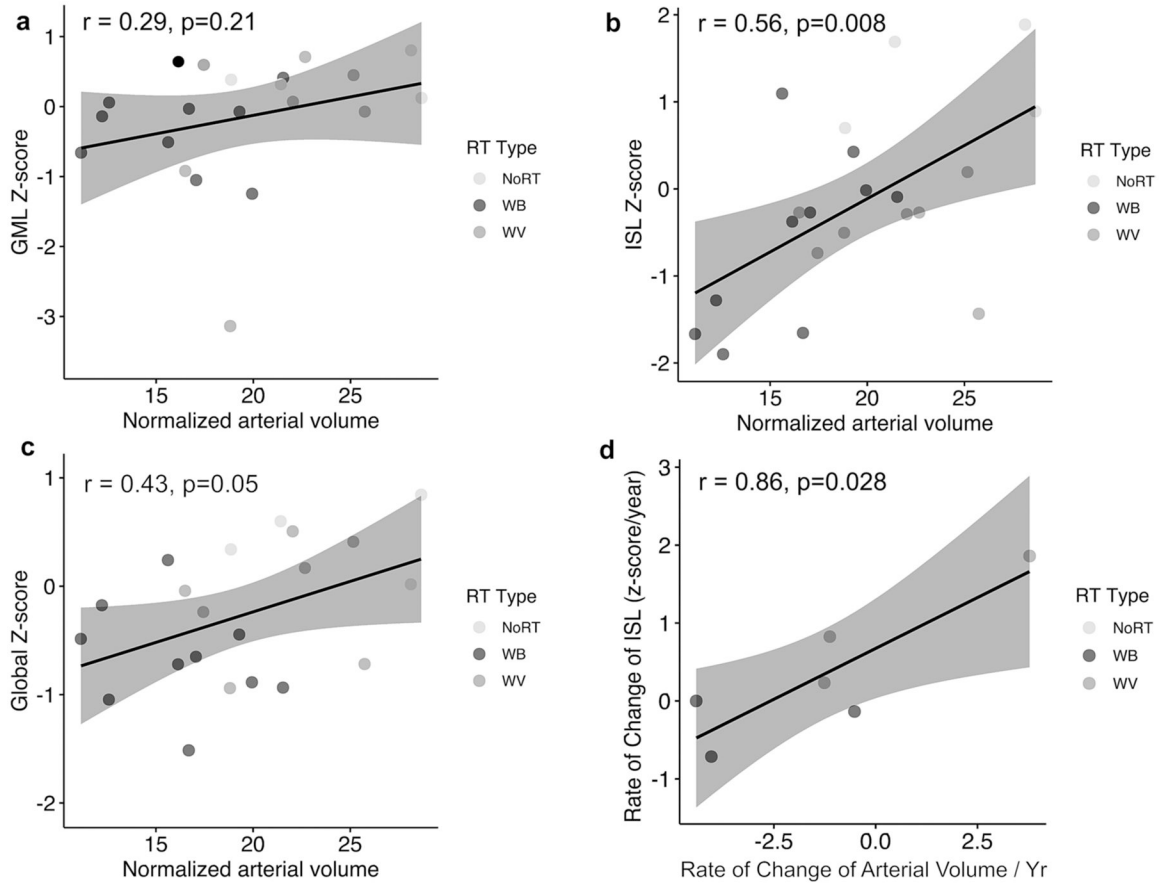

Fig. 4.

Correlation between normalized arterial volume and cognitive test z-scores. **a–c** Grotten maze learning (GML), International shopping list (ISL), and global z-scores in relation to normalized arterial volume; **d** Rate of change in ISL cognitive test scores plotted against rate change of normalized arterial volume in patients with serial scans. The shaded gray regions indicate 95% confidence interval

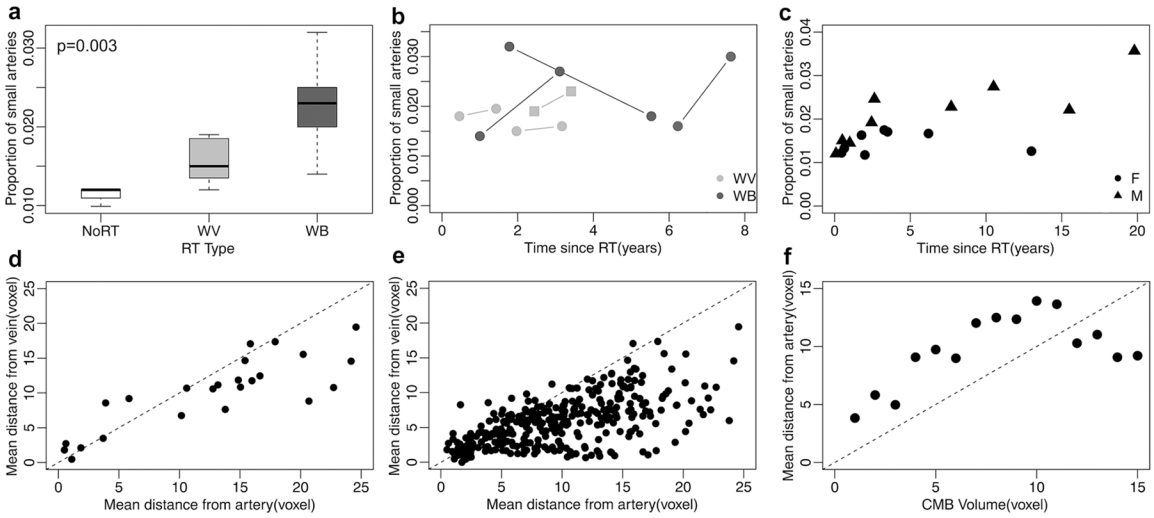

Fig. 5.

(Top row) Analysis of proportion of small vessels. **a** Distribution of proportion of small vessels in the different treatment groups; **b** Longitudinal differences in small vessel proportion in patients with serial scans; **c** Small vessel proportion plotted by gender as a function of time since RT. (Bottom row) Relationship of vessel locations to CMBs. **d** Correlation between the distance of a CMB from nearest artery and distance from the nearest vein for one patient; **e** Correlation between the distance of a CMB from the nearest artery and distance from nearest vein for all patients; **f** Mean distance from nearest artery as a function of individual CMB volume

Table 1

Patient demographics

Clinical/ demographic characteristics	Proportion of patients (N = 25)
	Median (Range)
Age at radiation therapy	12 (3–24)
Age at first scan	17 (10–25)
Follow-up time	3.29 (0.1–19.9)
Maximum radiation dose cGy	5445 (3000–5940)
	n (%)
Female	13 (52.0)
Left-handed	4 (16.0)
Race	
White	17 (68.0)
Asian	4 (16.0)
Black	1 (4.0)
Other	3 (12.0)
Histological diagnosis	
Medulloblastoma	11 (44.0)
Germinoma	5 (20.0)
Pilocytic astrocytoma	5 (20.0)
Other	4 (16.0)
Tumor location	
Posterior fossa	17 (68.0)
Ventricles	5 (20.0)
Supratentorial	3 (12.0)
Treatment	
Surgery	20 (80.0)
Chemotherapy	17 (68.0)
Radiation	19 (76.0)
Hydrocephalus	3 (12.0)